RSC Advances

PAPER

View Article Online
View Journal | View Issue

Cite this: *RSC Adv.*, 2017, **7**, 3853

Catalytic glycerol hydrogenolysis to 1,3-propanediol in a gas–solid fluidized bed

Mahesh Edake,*[a] Marjan Dalil,[a] Mohammad Jaber Darabi Mahboub,[a] Jean-Luc Dubois[b] and Gregory S. Patience[a]

Received 23rd November 2016
Accepted 26th November 2016

DOI: 10.1039/c6ra27248g

www.rsc.org/advances

Glycerol is a potential feedstock to produce 1,3-propanediol (1,3-PDO), which is a valuable commercial polyester monomer. Here, we report the gas-phase glycerol hydrogenolysis to 1,3-propanediol over Pt/WO_3/Al_2O_3 in a fluidized bed operating above 240 °C and at ambient pressure. Fluidized beds are ideal contactors for this reaction because the heat transfer rates are sufficiently high to vaporize glycerol thereby minimizing its combustion and thermal degradation. The yield of 1,3-PDO approached 14% after 2 h at 260 °C. The major co-products were 1,2-PDO (18%), 1-propanol (28%) and 2-propanol (15%). In the first step, glycerol may dehydrate to acrolein, followed by rehydration to 3-hydroxypropanal and then hydrogenation to 1,3-PDO. The concentrations of the by-products including acrolein, ethylene glycol, propane, and acetone increased with increasing temperature.

1 Introduction

Substituting fossil resources with renewable biomass to produce biofuels, chemicals, and bioplastics remains a priority for many countries.[1,2] Glycerol is a by-product of the transesterification of vegetable oils and animal fats to biodiesel.[3] As a consequence of government mandates to blend biodiesel with petro-diesel, glycerol has flooded traditional markets. These markets are incapable of absorbing the increased availability, so the price of glycerol has dropped.[4] The lower price makes it an attractive feedstock for other chemicals such as 1,2-propanediol (1,2-PDO) and 1,3-propanediol (1,3-PDO).[4,5]

1,3-PDO is a monomer for polytrimethylene terephthalate (PTT) together with terephthalic acid, that has unique properties for a wide range of end-uses; it has superior stretching and elastic recovery compared to nylon and that is difficult to achieve with other glycol based polyesters. The global value of the 1,3-PDO market was USD 310 million in 2014 and it is likely to reach USD 620 million by 2021 with a compound annual growth rate of 10.4% between 2014 and 2021.[6] Growing demand for PTT for end-uses in polyurethane, cosmetics, personal care and cleaning products[7] and increasing consumer preference for bio-based chemicals is expected to drive 1,3-PDO growth.[8] It can also be used as a constituent of engine coolants, food and beverages, de-icing fluids, heat-transfer fluids, and unsaturated polyester resins.

In 1990, Shell developed catalytic technology to convert ethylene oxide to PDO, which led to the Corterra® brand of thermoplastic polyesters. DuPont produces Sorona® brand polymers from PDO and terephthalic acid and they also partnered with Tate and Lyle to produce PDO from corn (*via* a fermentation process) and captured 89% of the total market in 2014.[9] Asia Pacific will be the fastest growing market, as many Chinese manufacturers will begin commercial production of 1,3-PDO in the coming years.

Yields of 1,2-PDO from glycerol hydrogenolysis are highest with bifunctional catalysts including a hydrogenation metal and an acid co-catalyst.[10–12] Producing 1,3-PDO is more challenging. The ratio of 1,2-PDO/1,3-PDO can be controlled by selectively cleaving the C–O bond of the primary or secondary hydroxyl groups of glycerol, which mostly depend on the type of catalyst. Chaminand[13] improved the 1,3-PDO yield at 200 °C and 80 bar adding H_2WO_4 to Rh/SiO_2 in a sulfolane medium. A Pt/WO_3/ZrO_2 catalyst achieved a 24% yield of 1,3-PDO in 1,3-dimethyl-2-imidazolidinone (DMI) as a solvent at 170 °C and 80 bar.[14] A Cu–$H_4SiW_{12}O_{40}/SiO_2$ catalyst reached a 27% yield of 1,3-PDO in the vapor phase and aqueous media at 5 bar and 210 °C. The 1,3-PDO yield over Pt deposited on a super-acid sulfated ZrO_2 support was 56% at 170 °C and 73 bar.[15] Environmental and economic concerns limit the use of organic solvents for a commercially viable process. Water is the ideal solvent for the process as glycerol is obtained in the aqueous phase after the transesterification reaction.[16]

Heterogeneous noble metals (Ir, Rh, or Pt) combined with oxophilic metals such as Mo, Re, and W catalyse glycerol hydrogenolysis in the aqueous phase.[17] Tomishige's group studied Rh–ReO_x/SiO_2 [18] and Ir/SiO_2 [19] catalytic systems for glycerol hydrogenolysis. H_2SO_4 modified the structure of the catalyst. The authors reported 38% 1,3-PDO selectivity at 120 °C and 80 bar over Ir/SiO_2. However, Re leached. More robust and

[a]*Department of Chemical Engineering, Polytechnique Montréal, Succ. CV Montréal, H3C 3A7 Québec, Canada. E-mail: maheshedake1@gmail.com; Tel: +1 514 243 4062*
[b]*ARKEMA, 420 Rue d'Estienne d'Orves, 92705 Colombes, France*

stable Pt–WO_3 based catalytic systems are options to avoid the leaching problems associated with Re. Recently, Priya *et al.* studied the hydrogenolysis of glycerol to 1,3-PDO over bimetallic catalysts supported on mordenite in the liquid phase. The maximum 1,3-PDO selectivity was 58.5%.[20,21] Selectivity of 1,3-PDO reached 32% with $Pt/WO_3/ZrO_2$ at 130 °C and 40 bar [16] but the highest selectivity to date was 66% (Table 1) with a Pt/WO_3/AlOOH catalyst.[22] Recent studies show that acrolein in an aqueous solution reacts to form 3-hydroxypropanal in a yield of 20%. Subsequently, hydrogen reacts with this intermediate to form 1,3-PDO.[23,24]

Homogeneous catalytic processes suffered from a catalyst separation problem and liquid phase heterogeneous catalytic processes need high pressure. We report the gas phase glycerol hydrogenolysis over a $Pt/WO_3/Al_2O_3$ catalyst in a fluidized bed at 260 °C and at atmospheric pressure, producing 14% 1,3-PDO. Glycerol conversion and PDOs' selectivity over the $Pt/WO_3/Al_2O_3$ catalyst are related to the physicochemical properties of the catalyst.

2 Experimental

2.1 Catalyst preparation

We prepared the $Pt/WO_3/Al_2O_3$ catalyst by an incipient wetness impregnation method. The support was Al_2O_3 with a particle size ranging from 100 μm to 150 μm, which is suitable to achieve uniform fluidization. Al_2O_3 (10 g) was impregnated with 20 wt% ammonium metatungstate ($(NH_4)_6(H_2W_{12}O_{40})\cdot nH_2O$) dissolved in 120 mL deionized water at 25 °C. The paste was dried at 120 °C overnight and then calcined in air at 550 °C at a heating rate of 2 °C min^{-1} for 4 h. In the second step, we loaded a mass fraction of 2% platinum on a supported tungsten oxide catalyst. The precursor was chloroplatinic acid hydrate, $H_2PtCl_6\cdot xH_2O$ (Sigma Aldrich 99.99%). The catalyst was dried and calcined under the same conditions as during the first step.

Table 1 State of the art catalysts for the selective hydrogenolysis of glycerol to 1,3-propanediol

Catalyst	P (bar)	T (°C)	Conv. gly (%)	Yield (%)
(Batch mode)				
$Pt/sulfated\text{-}ZrO_2$ [15]	73	170	67	56
$Ir/ReO_x–SiO_2$ [19]	80	120	50	25
$Pt/WO_3/ZrO_2$ [14]	80	170	86	24
$Pt/WO_3/ZrO_2$ [25]	55	170	46	13
Pt–Re/C[26]	40	170	45	13
$Rh–ReO_x/SiO_2$ [10]	80	120	79	11
$Pt/WO_3/ZrO_2/SiO_2$ [27]	55	180	15	7
Rh/C[13]	80	180	32	4
Rh/SiO_2 [28]	80	120	14	1
Pt–Re/C[29]	40	170	45	29
Pt/Al_2O_3 [30]	40	200	49	28
$Pt/WO_3/AlO_x$[22]	50	180	100	66
$Pt/m\text{-}WO_3$ [31]	55	180	18	39
(Fixed bed-continuous)				
$Pt/WO_3/ZrO_2$ [29]	40	130	70	32
$Cu/STA/SiO_2$ [16]	50	210	83	27
$Pt–STA/ZrO_2$ [32]	50	180	24	48
$Pt/WO_3/Zro_2$ [16]	40	130	70	46
$Pt/WO_x/ZrO_2$ [8]	50	180	54	52
$Pt/AlPO_4$ [33]	1	260	100	35
Ru/MCM[34]	1	280	62	20
Pt/Cu/Mor[20]	1	210	90	58.5
Pt/H-mordenite[21]	1	225	94.9	48.6

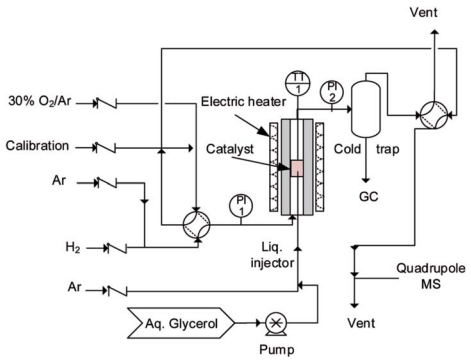

Fig. 1 Schematic of the experimental set-up.

2.2 Catalyst characterization

An Autosorb-1 system (Quantachrome Instruments) recorded the N_2 adsorption/desorption isotherms to give textural properties (surface area, pore volume, and pore size distributions). The samples were degassed at $T = 200$ °C under vacuum for 3 h. We calculated the specific surface area (SSA) following the multipoint Brunauer–Emmett–Teller (BET) procedure. A Philips Xpert diffractometer measured the X-ray diffraction pattern and crystallinity at room temperature (Cu anode ($K = 0.15406$ nm) at 50 kV voltage and 40 mA current). It scanned 2θ with a 0.020 step size. We identified the catalyst phases with JCPDS files. A JEOL JSM-7600TFE instrument scanned the surface of the catalysts and produced field emission scanning electron micrographs. We mounted the samples on an aluminum support covered with double-sided adhesive tape. A laser scattering PSD analyzer (LA-950, Horiba) measured the particle size distribution of the catalyst.

A TA-Q50 instrument recorded the thermogravimetric curves for the used catalysts. 20 mg samples of the catalysts were loaded onto a 10 μm aluminium crucible. The resolution of the balance was 0.1 μg. Prior to each experiment, we purged the samples with a 40 mL min^{-1} stream of nitrogen to remove volatiles adsorbed on the catalyst. Simultaneously, the furnace ramped the temperature at 10 °C min^{-1} up to 300 °C and remained constant for 15 min. We substituted nitrogen with

Table 2 Textural properties of the catalysts

Catalyst	SA, $m^2\ g^{-1}$	P_V, $cm^3\ g^{-1}$	P_d, Å
Al_2O_3	131	0.27	56
Pt/Al_2O_3	130	0.25	56
$Pt/WO_3/Al_2O_3$ (fresh)	120	0.22	48
$Pt/WO_3/Al_2O_3$ (used)	108	0.20	48

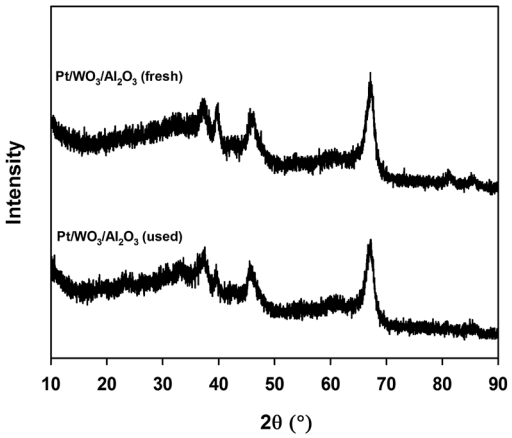

Fig. 2 XRD pattern for fresh and used $Pt/WO_3/Al_2O_3$.

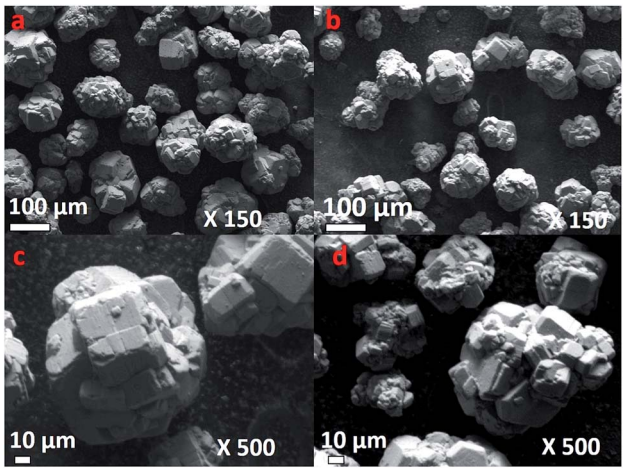

Fig. 3 FE-SEM micrographs of (a) fresh catalyst at ×150, (b) used catalyst after reaction ×150 (c) fresh catalyst at ×500, (d) used catalyst after reaction at ×500.

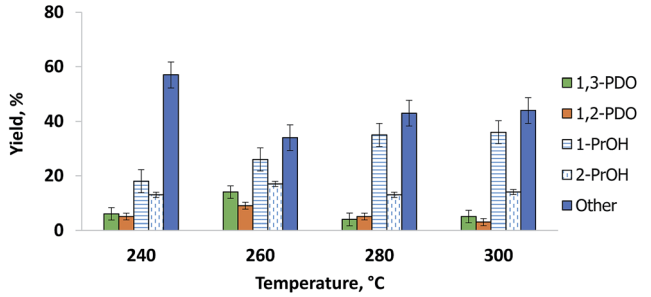

Fig. 4 Glycerol hydrogenolysis product distribution.

oxygen while heating to 550 °C with the same ramp conditions. A Platinel II thermocouple placed 2 mm above the sample pan monitored the temperature.

We evaluated the catalyst surface acidity by Fourier transform infrared spectroscopy with pyridine as the probe molecule. We placed samples in an infrared quartz cell, with CaF_2 windows and evacuated the chamber. Thereafter, we ramped the temperature in air to 150 °C. We degassed the cell at the same temperature for 1 h then introduced pyridine into the cell after returning to ambient temperature. All reported spectra were obtained by subtracting the spectrum of the activated catalyst (after pretreatment but before pyridine adsorption) from those after pyridine adsorption. We characterized the used catalyst after 2 h reaction time to evaluate the effect of time on stream. In this case, we took out the used catalyst from the reactor without regeneration.

2.3 Experimental set-up

An ideal fluidized bed operates isothermally and its radial concentration gradients are smaller than in packed beds. Mixing in micro-fluidized beds is inferior to larger reactors, since the bubbles are smaller, but we consider that the temperature

Table 3 Catalytic activity study of $Pt/WO_3/Al_2O_3$ during vapor phase glycerol hydrogenolysis

					Selectivity%				
Expt. no.	*T*, °C	H_2/gly ratio	WHSV, h^{-1}	Conversion%	1,3-PD	1,2-PD	1-PrOH	2-PrOH	Other[a]
1	240	18	0.09	76	6	5	16	14	59
2	240	28	0.14	78	7	6	18	13	56
3	240	14	0.14	78	7	5	19	13	56
4	260	9	0.09	98	12	13	23	15	37
5	260	14	0.14	98	13	11	25	16	35
6	260	18	0.09	99	13	12	26	15	34
7	260	28	0.14	99+	14	9	28	17	32
8	280	14	0.12	99+	6	5	36	13	40
9	280	18	0.09	99+	4	7	34	15	40
10	280	28	0.14	99+	4	4	37	13	42
11	280	14	0.14	99+	3	4	36	15	41
12	300	18	0.09	99+	4	3	36	15	42
13	300	9	0.09	99+	3	4	35	14	44
14	300	14	0.14	99+	4	3	37	13	43
15	300	28	0.14	99+	5	4	38	13	40

[a] Other: CO, CO_2, propane, acetone, methanol, propanal, acrolein, ethylene glycol, hydroxyacetone *etc.*

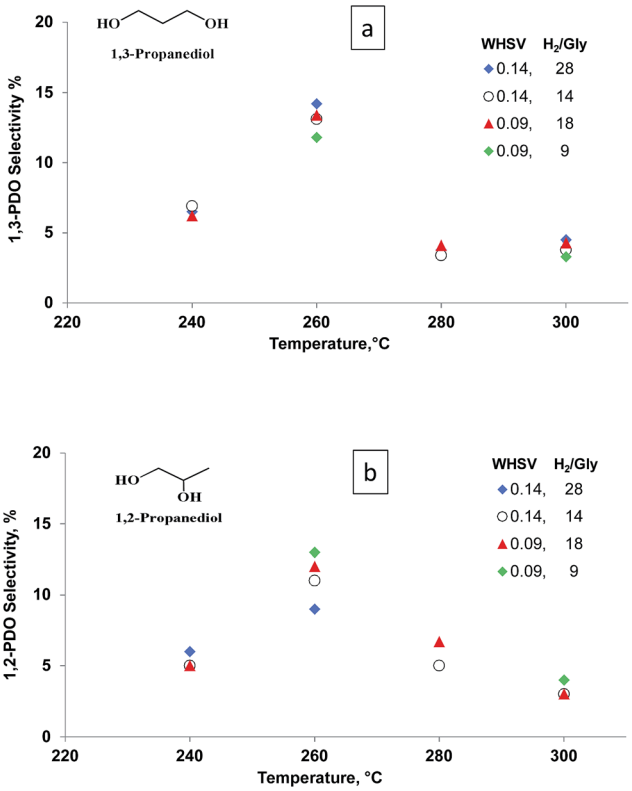

Fig. 5 Selectivity *vs.* temperature for (a) 1,3-PDO and (b) 1,2-PDO at WHSV = 0.09 to 0.14 h^{-1}, residence time = 0.43 s and 0.65 s and H_2/glycerol ratio = 9, 14, 18 and 28.

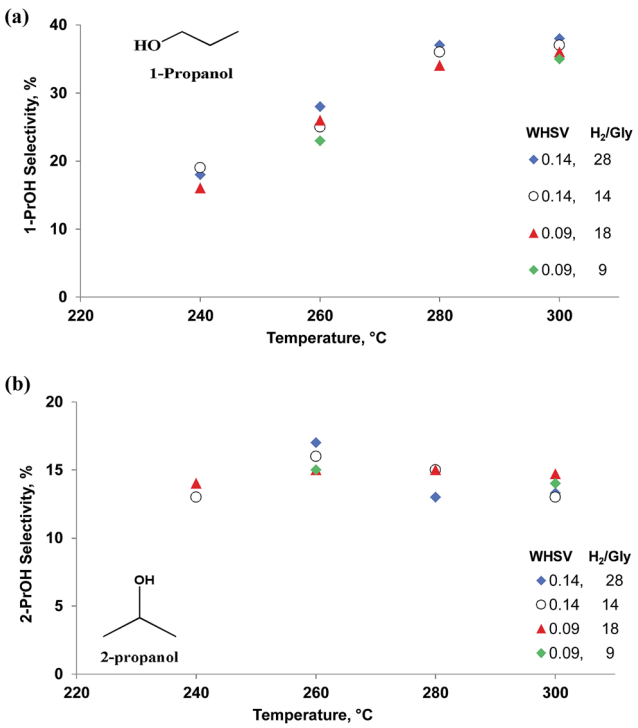

Fig. 6 Selectivity *vs.* temperature for (a) 1-PrOH and (b) 2-PrOH at WHSV = 0.09 to 0.14 h^{-1}, residence time = 0.43 s and 0.65 s and H_2/glycerol ratio = 9, 14, 18 and 28.

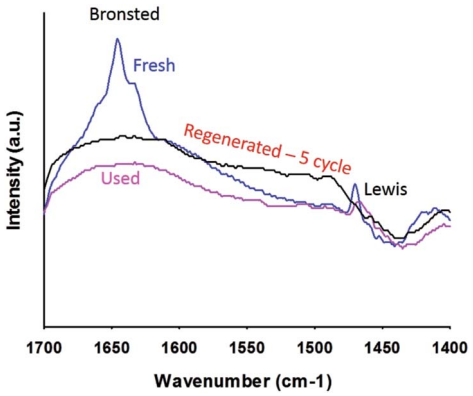

Fig. 7 Pyridine FTIR analysis of the fresh and used $Pt/WO_3/Al_2O_3$ catalyst.

Table 4 Mass loss of the $Pt/WO_3/Al_2O_3$ in a TGA fed with oxygen

Temp (°C)	H_2/gly	WHSV, h^{-1}	Wt. loss (%)
260	28	0.14	0.45
260	14	0.14	0.46
260	9	0.09	0.6

and concentration gradients of these beds are smaller than in comparable fixed bed reactors. Whilst the smaller bubbles in micro-fluidized beds reduce the overall mixing, they also reduce bypassing and for this reason conversion approaches 100% even in shallow beds of 10 mm. Atomizing gases and liquids into fluidized beds increases the heat transfer rates by orders of magnitude in comparison with fixed beds to derive the kinetics.[35,36]

We loaded 2.8 g of the catalyst into a 30 mm long quartz tube with a 7 mm inner diameter housed in a stainless steel tube to operate at high pressure (Fig. 1). A ceramic distributer in the middle of the tube distributed the gas uniformly across the diameter. A furnace heated the reactor to the set point (mostly 260 °C for the initial catalyst reduction with H_2). A type-K thermocouple inside the bed monitored its temperature. Bronkhorst mass flow controllers (from 200 mL min^{-1} to 1000 mL min^{-1}) maintained the gas flow rates. A syringe pump injected the aqueous glycerol solution (from 10% to 50%) *via* a 1/16″ tube from the bottom of the reactor. The injector passed through the gas distributor and entered the catalyst bed at a height of 10 mm. Prior to the activity test, pure H_2 reduced the catalyst with a flow of 50 mL min^{-1} at 350 °C for 1 h.

80 mL min^{-1} of H_2 fluidized the $Pt/WO_3/Al_2O_3$ catalyst (2.8 g for each test), while argon atomized the feed solution into the catalyst bed. All experiments lasted for 2 h. 30% oxygen in argon regenerated the catalyst at 550 °C.

Atomizing the liquid into uniform drops is important for operating the fluidized bed: large droplets cause the catalyst to agglomerate and block the injector and/or accumulate on top of the grid.[35,37] We examined several gas and liquid flow rates and glycerol concentrations to identify the optimum conditions.

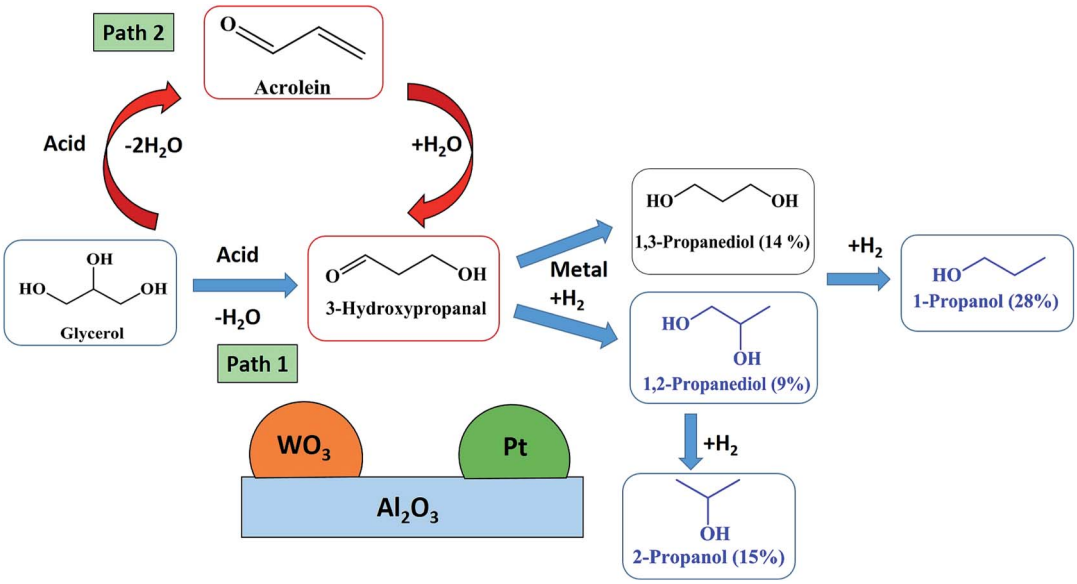

Fig. 8 Proposed reaction mechanism for glycerol hydrogenolysis to 1,3-PDO in a catalytic fluidized bed reactor at atmospheric pressure.

The total flow rate ($Q_{Ar} + Q_{H_2} + Q_{glycerol}$) changed from 140 mL min^{-1} to 210 mL min^{-1}, which corresponds to a velocity 3 or 5 times that of the minimum fluidization velocity (U_{mf}). To change the feed composition, we manipulated the feed rates of glycerol, hydrogen and Ar (the inert gas).

Therefore to reach the desired H_2/glycerol ratio, the mole fractions of the gases were modified according to the following:

– Ar/H_2/glycerol/water (%) = 3.2/81/9/1.8 to reach H_2/gly = 9.

– Ar/H_2/glycerol/water (%) = 3.8/84/6/1.2 to reach H_2/gly = 14.

– Ar/H_2/glycerol/water (%) = 4/90/5/1 to reach H_2/gly = 18.

– Ar/H_2/glycerol/water (%) = 3.6/92.4/3.3/0.7 to reach H_2/gly = 28.

A quench trapped all the condensables and the mist coming from the effluent gas and these were analyzed off-line using GC, GC-MS and HPLC. The gas products were monitored on-line using MS.

2.4 Product analysis

A Hiden QIC-200 quadrupole mass spectrometer monitored the partial pressure of the reaction products in real time. The mass spectrometer was calibrated before and after the experiment with a mix of Ar, CO, CO_2, H_2O, CH_4 and H_2 at two concentrations close to the concentration of the reactor effluent.

A Bruker GC (equipped with Hyesep Q, Molsieve 5A with FFAP columns) and a Varian HPLC (Metacarb 87H column) analysed the glycerol, 1,3-PDO, 1,2-PDO, 1-PrOH, 2-PrOH as well as other degradation products.

The conversion of glycerol ($X_{gly.}$) as well as selectivities toward products (S_p) were calculated as follows;

$$X_{gly.}\ (\text{mol}\%) = \frac{n^{in}_{gly.} - n^{out}_{gly.}}{n^{in}_{gly.}} \times 100 \quad (1)$$

$$S_p\ (\text{mol}\%) = \frac{n_p}{n^{in}_{gly.} - n^{out}_{gly.}} \times \frac{z_p}{z_{gly.}} \times 100 \quad (2)$$

Where: $n^{in}_{gly.}$ and $n^{out}_{gly.}$ are the molar flow rates of glycerol at the reactor's entrance and exit. In eqn (2), n_p is the molar stream of each product. z_p and $z_{gly.}$ represent the number of carbon atoms of the products and glycerol.

Table 5 Mechanistic pathway study by 1,3- and 1,2-PDO injection fed over Pt/WO_3/Al_2O_3 under the same reaction conditions

			Selectivity%						
Expt. no.	Reactant	Conversion%	1,3-PDO	1,2-PDO	1-PrOH	2-PrOH	C_3H_8	Acrolein	Other[a]
1	1,3-PDO	11	—	2	62	3	19	1	8
2	1,2-PDO	42	1	—	54	14	8	1	6
3	1-PrOH	32	0	2	—	2	23	2	8
4	2-PrOH	36	0	2	3	—	12	3	15
5	Acrolein	49	9	0	8	3	11	—	20
6	3-HPA	80	20	3	14	4	14	—	29

[a] Other: CO, CO_2, propanaldehyde, ethylene glycol, acetone *etc.*

3 Results and discussion

3.1 Physicochemical properties

The surface area of the Al_2O_3 support was 131 m^2 g^{-1}, with an average pore diameter of 56 Å, and total pore volume of 0.27 cm^3 g^{-1}. The surface area of the Al_2O_3 support was the same after Pt impregnation (Table 2). It dropped by 10% after we added WO_3 and another 10% after the reaction. The bulk support pore volume dropped from 0.27 cm^3 g^{-1} to 0.20 cm^3 g^{-1} due to tungsten oxide and platinum oxide species and/or coke blocking the Al_2O_3 pores.

The X-ray diffraction patterns of fresh and used $Pt/WO_3/Al_2O_3$ suggest that the synthesized catalyst is crystalline (Fig. 2). Both samples exhibit characteristic peaks of alumina. Peaks at 37.5°, 45.4°, 66.9° for 2θ values were attributed to crystalline Al_2O_3. Diffraction peaks attributable to crystalline WO_3 were absent indicating that the tungsten species are uniformly distributed. Diffraction peaks of metallic or oxidized Pt phases were absent, indicating that the metal was well dispersed across the surface of the support, which agrees with the literature studies.[22] After the reaction, the XRD diffraction pattern was unchanged.

The surface morphology of the calcined $Pt/WO_3/Al_2O_3$ was examined using FE-SEM (Fig. 3). A high magnification view of the catalyst shows that the particles were spheroidal. The surface was rough and the particles had a uniform diameter of approximately 80–120 μm. Catalyst assemblies were closely packed and no cracks were apparent on the grain surfaces.

Pyridine-IR analysis compared the strengths of the Lewis and Brønsted acid sites in $PtWO_3//Al_2O_3$. Liquid pyridine was adsorbed on the catalyst at room temperature and desorbed at 150 °C in a vacuum. The FT-IR spectra of the pyridine adsorbed catalysts were analyzed in the region of 1700 cm^{-1} to 1400 cm^{-1}. Bronsted (B) acid sites exhibited typical bands centered at 1640 cm^{-1} and 1540 cm^{-1}, and Lewis (L) acid sites at 1460 cm^{-1}. The fresh catalyst showed bands at 1454 cm^{-1} corresponding to Lewis acid sites and the other band observed at 1640 cm^{-1} is attributed to Brønsted acid sites. Although the total surface acidity is low, the Brønsted acid sites were the most apparent on $Pt/WO_3/Al_2O_3$.

3.2 Hydrogenolysis

Glycerol hydrogenolysis is a multi-step process in which an acid dehydrates glycerol, and a heterogeneous catalyst hydrogenates the intermediates to 1,2-PDO and 1,3-PDO. Generally, the 1,2-PDO yield is higher than that of 1,3-PDO. Maximizing 1,3-PDO selectivity requires Brønsted acid sites to selectively dehydrate the secondary carbon hydroxyl bond. The acid plays a decisive role in eliminating a hydroxyl group, and a fast sequential hydrogenation prevents further dehydration. In this study, we tested three catalysts while varying the feed composition and temperature to identify the optimum selectivity. We analyzed the product stream after a reaction time of 2 h. Here, we react glycerol in the vapour phase at 240 °C to 300 °C, at a hydrogen to glycerol ratio of 9 to 28, and WHSV between 0.09 and 0.14 h^{-1} and at ambient pressure (Table 3). Before atomizing the glycerol–water solution (a mass fraction of 20%), the catalyst was activated in a stream of H_2 at 350 °C for 2 h.

The catalyst produced the most 1,3-PDO at 260 °C. Both glycerol conversion and 1,3-PDO selectivity over the $Pt/WO_3/Al_2O_3$ catalyst depend on temperature,[16,25,32] (Fig. 4). Glycerol conversion was generally very high and exceeded 98% above 260 °C whereas 1,3-PDO selectivity reached a maximum at 260 °C. 1,3-PDO product selectivity doubled from 6% to over 14% when we increased the temperature from 240 to 260 °C. However, it decreased at higher temperatures presumably due to subsequent hydrogenation to 1-PrOH and 2-PrOH. Further increasing the temperature to 300 °C reduced the 1,3-PDO selectivity and increased by-products like 1,2-PDO, 1-PrOH and 2-PrOH. Similar results published over a bi-functional $Pt/WO_3/TiO_2/SiO_2$ catalyst in a batch reactor, explain how the increased temperature activates the terminal hydroxyl groups of glycerol.[25]

1,2-PDO formed in parallel with 1,3-PDO and its selectivity was lower at all temperatures except 280 °C (Fig. 4). As with 1,3-PDO, it reached a maximum selectivity of 13% at 260 °C. Other byproducts were 1-propanol and 2-propanol. We confirmed that these two compounds form directly from the hydrogenolysis of 1,3-PDO and 1,2-PDO. At 260 °C, 1-propanol selectivity was 25% and it increased with temperature to reach 38% at 300 °C. 2-Propanol selectivity increased less and reached a maximum of 17% at 260 °C.

The residence time varied from 0.43 s to 0.65 s (due to the change of total flow rate). However, in this study we conducted all experiments with a very high hydrogen flow, which is used as reactant as well as for fluidization purposes. Therefore the results of selectivity show that the products were independent of residence time changes.

Other by-products including propane, propanal, acrolein, ethylene glycerol, acetone, methanol and hydroxyacetone were also detected. The hydroxyacetone, acetone, methanol and propane concentrations were highest at 240 °C. CO and CO_2 formation increased with temperature from 240 °C to 300 °C.

Both glycerol conversion and product selectivities are independent of the H_2/glycerol ratio over the $Pt/WO_3/Al_2O_3$ (Fig. 5). Under each of the conditions, the selectivity to the diols and mono-alcohols were in the margin of error of the experimental data (Fig. 6). We varied the H_2/glycerol ratio from 9 to 29. We tested a WHSV of 0.09 h^{-1} and 0.14 h^{-1}.

3.3 Analysis of the used catalyst

The XRD patterns of the catalyst remained the same after the reaction as did the morphology and the crystalline size (Fig. 2). Crystalline Pt phases were absent after the reaction, which suggests that the Pt species were well dispersed while reacting (Fig. 2). The BET surface area of the catalyst decreased after the reaction from 120 m^2 g^{-1} to 107 m^2 g^{-1}. The total pore volume dropped from 0.22 cm^3 g^{-1} to 0.20 cm^3 g^{-1} (Table 2).

Based on FT-IR pyridine analysis both the concentration of the Lewis and Brønsted acid sites decreased after the reaction (Fig. 7). The ratio of Brønsted sites to Lewis acid cites was 1.18 after the reaction. Future work will examine more closely the change in acidity with time on-stream as well as during the

reoxidation process. Dalil *et al.*[38] have already demonstrated by FT-IR pyridine analysis on a WO_3/TiO_2 catalyst that the strong acid sites were changing for up to 14 h during for the dehydration of glycerol to acrolein. During this time the selectivity to acrolein increased while the by-products decreased and the medium acidic and basic sites decreased.

Air regenerated the used catalyst in a TGA from which we derived the mass loss due to carbon that accumulated during the reaction (Table 4). It was relatively insensitive to H_2/gly: the ratio changed by a factor of 3 but only 25% more carbon evolved from the catalyst. The catalyst has a small proportion of basic sites that became coked with time but the catalyst was stable over all of the conditions. The pore volume and surface area changed slightly, which confirms that the catalyst is stable and carbon builds up on a small fraction of the catalyst.

3.4 Reaction mechanism

The two step dehydration–hydrogenation pathway to convert glycerol to 1,3-PDO is widely accepted.[22] In the first step, glycerol dehydrates to 3-hydroxypropanal (3-HPA) and then hydrogenates in a second step to 1,3-PDO (Fig. 8, Path 2). Over acidic catalysts, the double dehydration of glycerol gives acrolein, which could be the precursor for 3-hydroxypropanaldehyde (3-HPA) after rehydration (Fig. 8, Path 1). The second dehydration to acrolein and the rehydration would be an equilibrium, which depends on water partial pressure and temperature. This equilibrium stage is important: PDO selectivity increases with higher H_2O partial pressure, and lower temperature (to limit the second dehydration) but this will also affect the first dehydration. A detailed mechanism of acrolein formation with 3-HPA as an intermediate has been stated in our recently published work on glycerol dehydration over a WO_3–TiO_2 catalyst.[37]

The reaction mechanism includes 3-steps: (1) double dehydration of glycerol to acrolein, (2) rehydration of acrolein to 3-HPA, (3) hydrogenation of 3-HPA to 1,3-PDO (Fig. 8, Path 1).

We validated this mechanism by feeding intermediate products—1,3-PDO, 1,2-PDO, 1-PrOH, 2-PrOH, and acrolein—to the $Pt/WO_3/Al_2O_3$ catalyst under the same reaction conditions (Table 5). 1,3-PDO was less active than 1,2-PDO, the propanols, and glycerol but its selectivity to 1-PrOH was 62% *versus* 54%. This result accounts for the yield of 1,3-PDO being higher *versus* 1,2-PDO during glycerol hydrogenolysis. The selectivity of 1-PrOH from 1,2-PDO was higher than for 2-PrOH. During glycerol hydrogenolysis, the 1-PrOH yield continued to increase with temperature while the 2-PrOH reached a maximum selectivity of 17% at 260 °C and dropped slightly to 15% at 280 °C and 300 °C (Fig. 6). These experiments demonstrate that glycerol hydrogenolysis follows a consecutive reaction pathway. To achieve high 1,3-PDO selectivity, we must suppress the consecutive reaction to 1-PrOH but more importantly the parallel reaction to 1,2-PDO. Also, 2-PrOH, propanal, acetone and ethylene glycol were produced in lower quantities from 1,3-PDO *versus* 1,2-PDO.

Acrolein hydrogenolysis produced 9% 1,3-PDO, which confirms that 3-HPA is the probable intermediate for the diols. We observed the same products during the hydrogenolysis experiments with glycerol by GC and GC-MS: 1-PrOH, propane and CO, CO_2, propanal, ethylene glycol and acetone.

4 Conclusions

We demonstrate a catalyst system—$Pt/WO_3/Al_2O_3$—that converts glycerol to 1,3-PDO and 1,2-PDO in the gas phase at ambient pressure and elevated temperatures in a fluidized bed reactor. The maximum yield of 1,3-PDO, the desired product, was 14%. It decreased with increasing temperature and produced more 1-PrOH. The other by-products were 2-PrOH, propanal, methanol, ethylene glycol, acetone, CO and CO_2. The consecutive reaction rate of 1,3-PDO to 1-PrOH is low; the most important factor for increasing selectivity is to reduce the parallel reaction to 1,2-PDO. A proposed mechanism pathway shows that the reaction occurs *via* a double dehydration of glycerol – rehydration of acrolein – followed by metal supported hydrogenation to give 1,3-PDO.

Acknowledgements

The authors would like to acknowledge CRIBIQ and MITACS (Canada) for their partial financial support of this study.

References

1 P. Gallezot, *Chem. Soc. Rev.*, 2012, **41**, 1538–1558.
2 C. O. Tuck, E. Perez, I. Horvath, R. Sheldon and M. Poliakoff, *Science*, 2012, **337**, 695–699.
3 D. Boffito, C. Neagoe, M. Edake, B. Pastor-Ramirez and G. Patience, *Catal. Today*, 2014, **237**, 13–17.
4 I. Gandarias, J. Requies, P. Arias, U. Armbruster and A. Martin, *J. Catal.*, 2012, **290**, 79–89.
5 A. Ruppert, K. Weinberg and R. Palkovits, *Angew. Chem., Int. Ed.*, 2012, **51**, 2564–2601.
6 PRNewswire, 1,3-propanediol market worth $621.2 million by 2021, http://www.prnewswire.com/news-releases/13-propanediol-market-worth-6212-million-by-2021-287634261.html, 2015.
7 C. Zhou, J. Beltramini, Y. X. Fan and G. Q. Lu, *Chem. Soc. Rev.*, 2008, **37**, 527–549.
8 D. T. U. Hanefeld, *ChemSusChem*, 2011, **4**, 1017–1034.
9 G. Kraus, *Clean: Soil, Air, Water*, 2008, **36**, 648–651.
10 Y. Shinmi, S. Koso, T. Kubota, Y. Nakagawa and K. Tomishige, *Appl. Catal., B*, 2010, **94**, 318–326.
11 M. Akiyama, S. Sato, R. Takahashi, K. Inui and M. Yokota, *Appl. Catal., A*, 2009, **371**, 60–66.
12 Z. Yuan, L. Wang, J. Wang, S. Xia, P. Chen, Z. Hou and X. Zheng, *Appl. Catal., B*, 2011, **101**, 431–440.
13 J. Chaminand, L. Djakovitch, P. Gallezot, P. Marion, C. Pinel and C. Rosier, *Green Chem.*, 2004, **6**, 359–361.
14 T. Kurosaka, H. Maruyama and Y. Sasaki, *Catal. Commun.*, 2008, **9**, 1360–1363.
15 J. Oh, S. Dash and H. Lee, *Green Chem.*, 2011, **13**, 2004–2007.
16 L. Qin, M. J. Song and C. Chen, *Green Chem.*, 2010, **12**, 1466–1472.

17 M. Chiaand, T. Pagan, D. Hibbitts, Q. Tan, H. N. Pham, A. K. Datye, M. Neuroc, R. J. Davis and J. A. Dumesic, *J. Am. Chem. Soc.*, 2011, **133**, 12675–12689.
18 S. Koso, H. Watanabe, K. Okumura, Y. Nakagawa and K. Tomishige, *Appl. Catal., B*, 2012, **111–112**, 27–37.
19 Y. Nakagawa, X. Ning, Y. Amada and R. Tomishige, *Appl. Catal., A*, 2012, **433–434**, 128–134.
20 S. S. Priya, P. Bhanuchander, V. P. Kumar, S. K. Bhargava and K. V. R. Chary, *Ind. Eng. Chem. Res.*, 2016, **55**, 4461–4472.
21 S. S. Priya, P. Bhanuchander, V. P. Kumar, D. K. Dumbre, S. R. Periasamy, S. K. Bhargava, M. L. Kantam and K. V. R. Chary, *ACS Sustainable Chem. Eng.*, 2016, **4**, 1212–1222.
22 R. Arundhathi, T. Mizugaki, T. Mitsudome, K. Jitsukawa and K. Kaneda, *ChemSusChem*, 2013, **6**, 1345–1347.
23 V. Resch and U. Hanefeld, *Catal. Sci. Technol.*, 2015, **5**, 1385–1399.
24 D. Arntz, A. Fischer, M. Hopp, S. Jacobi, J. Sauer, T. Ohara, T. Sato, N. Shimizu and H. Schwind, *Ullmann's Encyclopedia of Industrial Chemistry*, 2007, vol. 1, pp. 329–342.
25 L. Gong, Y. Lu, Y. Ding, R. Lin, J. Li and W. Chen, *Chin. J. Catal.*, 2009, **30**, 1189–1191.
26 O. Daniel, A. DeLaRiva, E. L. Kunkes, A. K. Datye, J. A. Dumesic and R. J. Davis, *ChemCatChem*, 2010, **2**, 1107–1114.
27 A. Shimao, S. Koso, N. Ueda, Y. Shinmi, I. Furikado and K. Tomishige, *Chem. Lett.*, 2009, **38**, 540–541.
28 I. Furikado, T. Miyazawa, S. Koso, A. Shimao, K. Kunimori and K. Tomishige, *Green Chem.*, 2007, **9**, 582–588.
29 L. Huang, Y. Zhu, H. Zheng, G. Ding and Y. Li, *Catal. Lett.*, 2009, **131**, 312–320.
30 T. Dam, D. Kristina, K. Freek and U. Hanefeld, *ChemCatChem*, 2013, **5**, 497–505.
31 L. Liu, Y. Zhang, A. Wang and T. Zhang, *Chin. J. Catal.*, 2012, **33**, 1257–1261.
32 C. H. Zhou, H. Zhao, D. S. Tong, L. M. Wu and W. H. Yu, *Catal. Rev.*, 2013, **55**, 369–453.
33 S. Priya, V. Kumar, M. Kantam, S. Bhargava and K. Chary, *RSC Adv.*, 2014, **4**, 51893–51903.
34 P. Vanama, A. Kumar, S. Ginjupalli and K. Chary, *Catal. Today*, 2015, **250**, 226–238.
35 M. J. D. Mahboub, S. Lotfi, J.-L. Dubois and G. S. Patience, *Catal. Sci. Technol.*, 2016, **6**, 6525–6535.
36 M. J. D. Mahboub, M. Rostamizadeh, J.-L. Dubois and G. S. Patience, *RSC Adv.*, 2016, **6**, 114–123.
37 M. Dalil, D. Carnevali, J. Dubois and G. Patience, *Chem. Eng. J.*, 2015, **270**, 557–563.
38 M. Dalil, D. Carnevali, M. Edake, A. Auroux, J.-L. Dubois and G. S. Patience, *J. Mol. Catal. A: Chem.*, 2016, **421**, 146–155.

